

NEW NEUTRINO MASS BOUNDS FROM SLOAN DIGITAL SKY SURVEY III DATA RELEASE 8 PHOTOMETRIC LUMINOUS GALAXIES

ROLAND DE PUTTER^{1,2}, OLGA MENA², ELENA GIUSARMA², SHIRLEY HO^{3,4}, ANTONIO CUESTA⁵, HEE-JONG SEO^{3,6}, ASHLEY J. ROSS⁷, MARTIN WHITE^{3,8}, DMITRY BIZYAEV⁹, HOWARD BREWINGTON⁹, DAVID KIRKBY¹⁰, ELENA MALANUSHENKO⁹, VIKTOR MALANUSHENKO⁹, DANIEL ORAVETZ⁹, KAIKE PAN⁹, WILL J. PERCIVAL⁷, NICHOLAS P. ROSS³, DONALD P. SCHNEIDER^{11,12}, ALAINA SHELDEN⁹, AUDREY SIMMONS⁹, STEPHANIE SNEDDEN⁹

(Dated: October 29, 2018)
Draft version October 29, 2018

ABSTRACT

We present neutrino mass bounds using 900,000 luminous galaxies with photometric redshifts measured from Sloan Digital Sky Survey III Data Release Eight (SDSS DR8). The galaxies have photometric redshifts between $z = 0.45$ and $z = 0.65$, and cover 10,000 square degrees and thus probe a volume of $3h^{-3}\text{Gpc}^3$, enabling tight constraints to be derived on the amount of dark matter in the form of massive neutrinos. A new bound on the sum of neutrino masses $\sum m_\nu < 0.26$ eV, at 95% confidence level (CL), is obtained after combining our sample of galaxies, which we call "CMASS", with WMAP 7 year Cosmic Microwave Background (CMB) data and the most recent measurement of the Hubble parameter from the Hubble Space Telescope (HST). This constraint is obtained with a conservative multipole range choice of $30 < \ell < 200$ in order to minimize non-linearities, and a free bias parameter in each of the four redshift bins. We study the impact of assuming this linear galaxy bias model using mock catalogs, and find that this model causes a small ($\sim 1 - 1.5\sigma$) bias in $\Omega_{\text{DM}}h^2$. For this reason, we also quote neutrino bounds based on a conservative galaxy bias model containing additional, shot noise-like free parameters. In this conservative case, the bounds are significantly weakened, e.g. $\sum m_\nu < 0.36$ eV (95% confidence level) for WMAP+HST+CMASS ($\ell_{\text{max}} = 200$). We also study the dependence of the neutrino bound on multipole range ($\ell_{\text{max}} = 150$ vs $\ell_{\text{max}} = 200$) and on which combination of data sets is included as a prior. The addition of supernova and/or Baryon Acoustic Oscillation data does not significantly improve the neutrino mass bound once the HST prior is included.

A companion paper (Ho et al. 2012) describes the construction of the angular power spectra in detail and derives constraints on a general cosmological model, including the dark energy equation of state w and the spatial curvature Ω_K , while a second companion paper Seo et al. (2012) presents a measurement of the scale of baryon acoustic oscillations from the same data set. All three works are based on the catalog by Ross et al. (2011).

1. INTRODUCTION

During the last several years, experiments involving solar, atmospheric, reactor and accelerator neutrinos have adduced robust evidence for flavor change, implying non-zero neutrino mass, see Ref. Gonzalez-Garcia & Maltoni (2008) and references therein. The most economical de-

scription of the neutrino oscillation phenomena requires at least two massive neutrino mass eigenstates to explain the two mass differences¹³, $\Delta m_{12}^2 = 7.59 \cdot 10^{-5}$ eV² and $\Delta m_{23}^2 = 2.5 \cdot 10^{-3}$ eV² Schwetz et al. (2011); Fogli et al. (2011), which drive the solar and atmospheric transitions. Despite the remarkable success of past and present oscillation experiments, and the promising prospects for future searches, the individual neutrino masses and the Dirac versus Majorana neutrino character are key questions that continue to be unanswered by oscillation experiments.

Direct information on the absolute scale of neutrino masses can be extracted from kinematical studies of weak decays producing neutrinos. The present upper bound on the electron-neutrino mass from tritium beta-decay experiments is 2 eV (95% confidence level (CL)) Lobashev (2003); Eitel (2005), and in the future the KATRIN experiment is expected to be sensitive to electron-neutrino masses approaching 0.2 eV (90% CL) Otten & Weinheimer (2008). Searches for the Majorana neutrino nature involve neutrinoless double beta decay $\beta\beta(0\nu)$, a rare and as yet unobserved transition between two nu-

¹ ICC, University of Barcelona (IEEC-UB), Marti i Franques 1, Barcelona 08028, Spain

² Instituto de Fisica Corpuscular, University of Valencia-CSIC, Spain

³ Lawrence Berkeley National Laboratory, 1 Cyclotron Road, Berkeley, CA 94720

⁴ Carnegie Mellon University, Physics Department, 5000 Forbes Ave, Pittsburgh, PA 15213

⁵ Yale University, New Haven, CT

⁶ Berkeley Center for Cosmological Physics, University of California, Berkeley, CA 94720

⁷ Institute of Cosmology & Gravitation, Dennis Sciama Building, University of Portsmouth, Portsmouth PO1 3FX, UK

⁸ Departments of Physics and Astronomy, University of California, Berkeley, CA 94720

⁹ Apache Point Observatory, P.O. Box 59, Sunspot, NM 88349-0059, USA

¹⁰ Department of Physics and Astronomy, University of California, Irvine, CA 92697

¹¹ Department of Astronomy and Astrophysics, The Pennsylvania State University, University Park, PA 16802

¹² Institute for Gravitation and the Cosmos, The Pennsylvania State University, University Park, PA 16802

¹³ Neutrino oscillations are described by mass squared differences and not by the absolute values of the mass eigenstates

clei. Observational upper limits on $\beta\beta(0\nu)$ rates provide an upper bound on the so-called effective Majorana mass of the electron neutrino, $\langle m_{\text{eff}} \rangle < 0.3 - 1.0$ eV, bound which would only apply if neutrinos are Majorana particles Gomez-Cadenas et al. (2011). Forthcoming $\beta\beta(0\nu)$ experiments aim for sensitivity approaching $\langle m_{\text{eff}} \rangle < 0.05$ eV Gomez-Cadenas et al. (2011).

Cosmology provides one of the means to tackle the absolute scale of neutrino masses. Some of the earliest cosmological bounds on neutrino masses followed from the requirement that massive relic neutrinos, present today in the expected numbers, do not saturate the critical density of the Universe, i.e., that the neutrino mass energy density given by

$$\Omega_\nu = \frac{\sum m_\nu}{93.1 h^2 \text{eV}} \quad (1)$$

satisfies $\Omega_\nu \leq 1$. The Universe therefore offers a new laboratory for testing neutrino masses and neutrino physics. Accurate measurements of the Cosmic Microwave Background (CMB) temperature and polarization anisotropy from satellite, balloon-borne and ground-based experiments have fully confirmed the predictions of the standard cosmological model and allow us to weigh neutrinos Lesgourgues & Pastor (2006). Indeed, neutrinos can play a relevant role in large-scale structure formation and leave key signatures in several cosmological data sets. More specifically, the amount of primordial relativistic neutrinos changes the epoch of matter-radiation equality, leaving an imprint on CMB anisotropies. After becoming non-relativistic, their free-streaming nature damps power on small scales, suppressing the growth of matter density fluctuations and thus affecting both the CMB and galaxy clustering observables in the low-redshift universe Lesgourgues & Pastor (2006). Measurements of all of these observations have been used to place new bounds on neutrino physics from cosmology Elgaroy et al. (2002); Spergel et al. (2003); Hannestad (2003); Allen et al. (2003); Tegmark et al. (2004); Barger et al. (2004); Hannestad & Raffelt (2004); Crotty et al. (2004); Seljak et al. (2005); Elgaroy & Lahav (2005); Hannestad (2005); Goobar et al. (2006); Spergel et al. (2007); Seljak et al. (2006); Fogli et al. (2008); Komatsu et al. (2009); Reid et al. (2010); Reid et al. (2010a); Thomas et al. (2010); Reid et al. (2010b); Komatsu et al. (2011); Saito et al. (2011); Riemer-Sørensen et al. (2011); Benson et al. (2011), with a current limit on the sum of neutrino masses $\Sigma m_\nu \lesssim 0.6$ eV at 95% CL (e.g. Reid et al. (2010)), depending on the precise combination of data sets and on the underlying cosmological model.

We present here neutrino mass bounds from the final imaging data set of the Sloan Digital Sky Survey (SDSS-III) York et al. (2000), using the photometric redshift catalog of Ross et al. (2011). We consider the CMASS sample White et al. (2011) of luminous galaxies of SDSS DR8 Aihara et al. (2011), the eighth data release of SDSS and the first data release of the Baryon Oscillation Spectroscopic Survey (BOSS) Eisenstein et al. (2011), with photometric redshifts $z = 0.45 - 0.65$. This sample covers an area of approximately 10,000 square degrees and consists of 900,000 galaxies. It is thus the largest sample of luminous galaxies so far and promises strong constraints on the neutrino proper-

ties (see Thomas et al. (2010) for an analysis of a slightly smaller SDSS photometric sample).

We derive neutrino constraints from the angular power spectra of the galaxy density at different redshifts, in combination with priors from the CMB and from measurements of the Hubble parameter, supernovae distances and the BAO scale. The spectra and the analysis of a minimal Λ CDM cosmology are described in detail in our companion paper Ho et al. (2012) and the measurement of the BAO scale from the spectra is presented in a separate companion paper Seo et al. (2012). We will often refer to these works for details and focus here on the neutrino bound.

The structure of the paper is as follows. In section 2, we describe the data set and the derived angular spectra. We then discuss our theoretical model for the spectra and their cosmology dependence in section 3. In section 4 we explain the specific signature of neutrino mass on galaxy clustering data. We test our model for the angular power spectra against mock data in section 5 and present the constraints on the sum of the neutrino masses and other parameters for several data combinations in section 6. Finally, we discuss these results and conclude in section 7.

2. DATA

The data and the method for obtaining angular spectra have been described in detail in Ref. Ross et al. (2011) and in Ho et al. (2012). Here we provide a brief description of the main properties and refer the reader to those papers for details. Our galaxy sample is obtained from imaging data from DR8 Aihara et al. (2011) of SDSS-III York et al. (2000). This survey mapped about 15,000 square degrees of the sky in five pass bands (u, g, r, i and z) Fukugita et al. (1996) using a wide field CCD camera Gunn et al. (1998) on the 2.5 meter Sloan telescope at Apache Point Observatory Gunn et al. (2006) (the subsequent astrometric calibration of these imaging data is described in Pier et al. (2003)). A sample of 112,778 galaxy spectra from BOSS Eisenstein et al. (2011) were used as a training sample for the photometric redshift catalog, as described in Ross et al. (2011).

We focus on the approximately stellar mass-limited CMASS sample of luminous galaxies, detailed in White et al. (2011), which are divided into four photometric redshift bins, $z_{\text{photo}} = 0.45 - 0.5 - 0.55 - 0.6 - 0.65$. The photometric redshift error lies in the range $\sigma_z(z) = 0.04 - 0.06$, increasing from low to high redshift. Figure 1 shows the estimated true redshift distribution of each bin, determined using the methods described in section 5.3 of Ross et al. (2011).

The calculation of the angular power spectrum for each bin is described in detail in our companion paper Ho et al. (2012) and uses the optimal quadratic estimator (OQE) method outlined in Seljak (1998); Tegmark et al. (1998); Padmanabhan et al. (2003, 2007). The four power spectra are binned in ℓ space with a typical wave band width of $\Delta\ell = 10$. The expectation value of the power spectrum in a wave band is a convolution of the true power spectrum with a window function of width roughly equal to the typical wave band width. Examples of these window functions are shown in Fig. 3 of the companion paper Seo et al. (2012). When fitting the data to the underlying theoretical model, we always apply these window func-

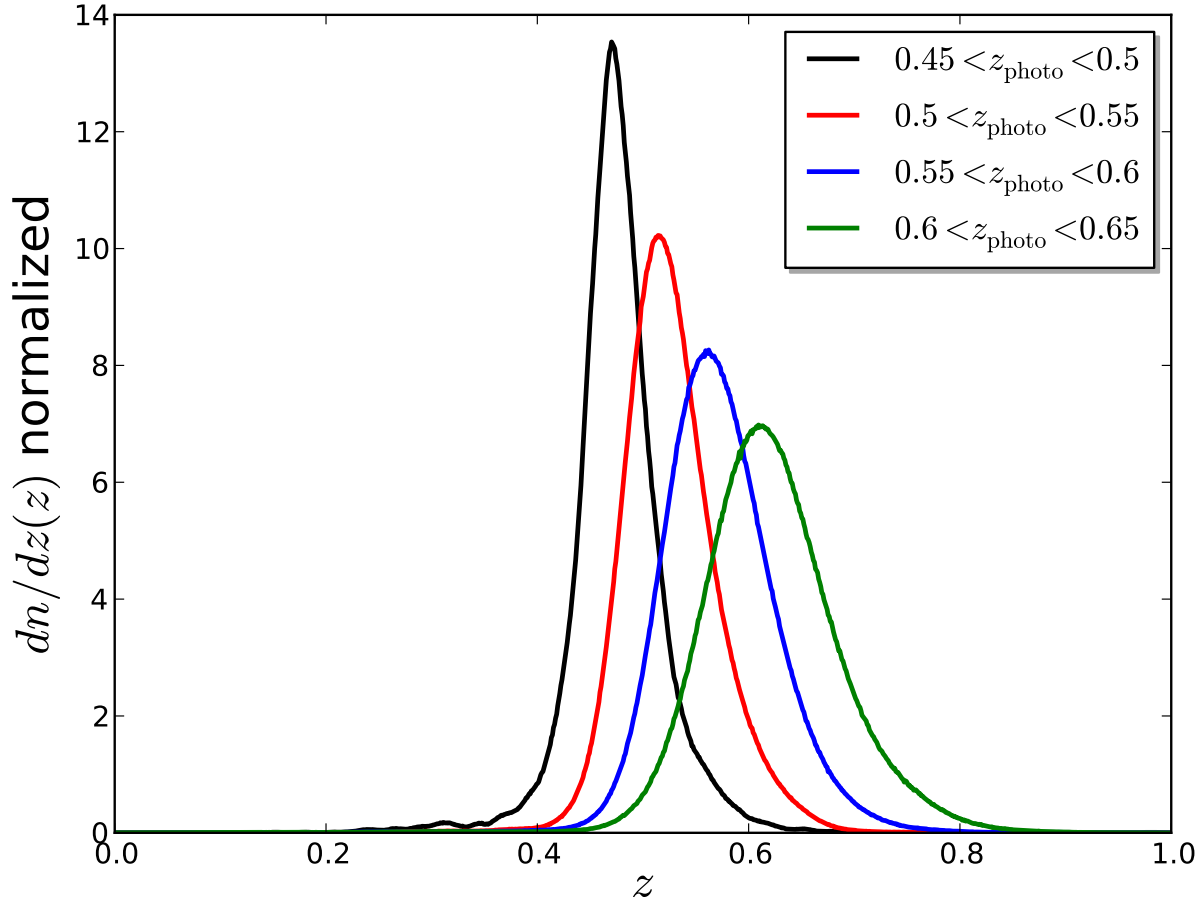


FIG. 1.— Normalized true redshift distribution of CMASS galaxies in four photometric redshift bins. The number of galaxies in each bin is 214971, 258736, 248895 and 150319 (from low to high redshift).

tions to the theoretical power spectra before calculating the likelihood relative to the data.

The four power spectra are plotted with their error bars in Fig. 2. The solid curves represent theoretical power spectra based on several assumptions. These power spectra will be discussed in detail in section 3. Since the low ℓ wave bands are more prone to systematics Ross et al. (2011), we are conservative and do not consider bands with $\ell < 30$ in our analysis. We shall apply cuts at $\ell_{\max} = 150$ and 200 in order to suppress uncertainties from non-linear corrections to the modeled power spectra, as discussed in the following sections. The median redshift ($z \approx 0.55$) contributions to these maximum angular modes arise from three-dimensional modes with wave vectors $k \approx 0.10h\text{Mpc}^{-1}$ and $k \approx 0.14h\text{Mpc}^{-1}$, respectively. We thus use 17 (12) data points per redshift slice for $\ell_{\max} = 200$ (150).

3. MODELING THE ANGULAR POWER SPECTRA

The galaxy overdensity in the i -th redshift bin can be expanded in terms of spherical harmonics,

$$\delta_g^{(i)}(\hat{n}) = \sum_{\ell m} a_{\ell m}^{(i)} Y_{\ell m}(\hat{n}), \quad (2)$$

so that the angular power (and cross) spectra are defined as

$$\langle a_{\ell m}^{(i)} a_{\ell' m'}^{(j)*} \rangle \equiv C_{\ell}^{(ij)} \delta_{\ell\ell'}^{\text{K}} \delta_{mm'}^{\text{K}}, \quad (3)$$

where δ_{ij}^{K} is the Kronecker delta function. As mentioned in the previous section, we do not estimate our spectra by directly transforming the observed density field to harmonics space, but use instead the optimal quadratic estimator technique. To constrain the sum of the neutrino masses and other cosmological parameters, the observed spectra are compared to a cosmology dependent model, which we now describe.

The galaxy overdensity on the sky is a line-of-sight projection of the three-dimensional redshift space galaxy overdensity $\delta_g(d(z) \hat{\mathbf{n}}, z)$,

$$\delta_g^{(i)}(\hat{\mathbf{n}}) = \int dz g_i(z) (\delta_g(d(z) \hat{\mathbf{n}}, z) - (H(z))^{-1} \hat{\mathbf{n}} \cdot \nabla(\hat{\mathbf{n}} \cdot \mathbf{v}(d(z) \hat{\mathbf{n}}, z))), \quad (4)$$

where

$$g_i(z) = \frac{dn_i/dz(z)}{\int dz' dn_i/dz(z')} \quad (5)$$

is the normalized redshift distribution of galaxies in bin i (with $dn_i/dz(z)$ the number of galaxies per steradian per

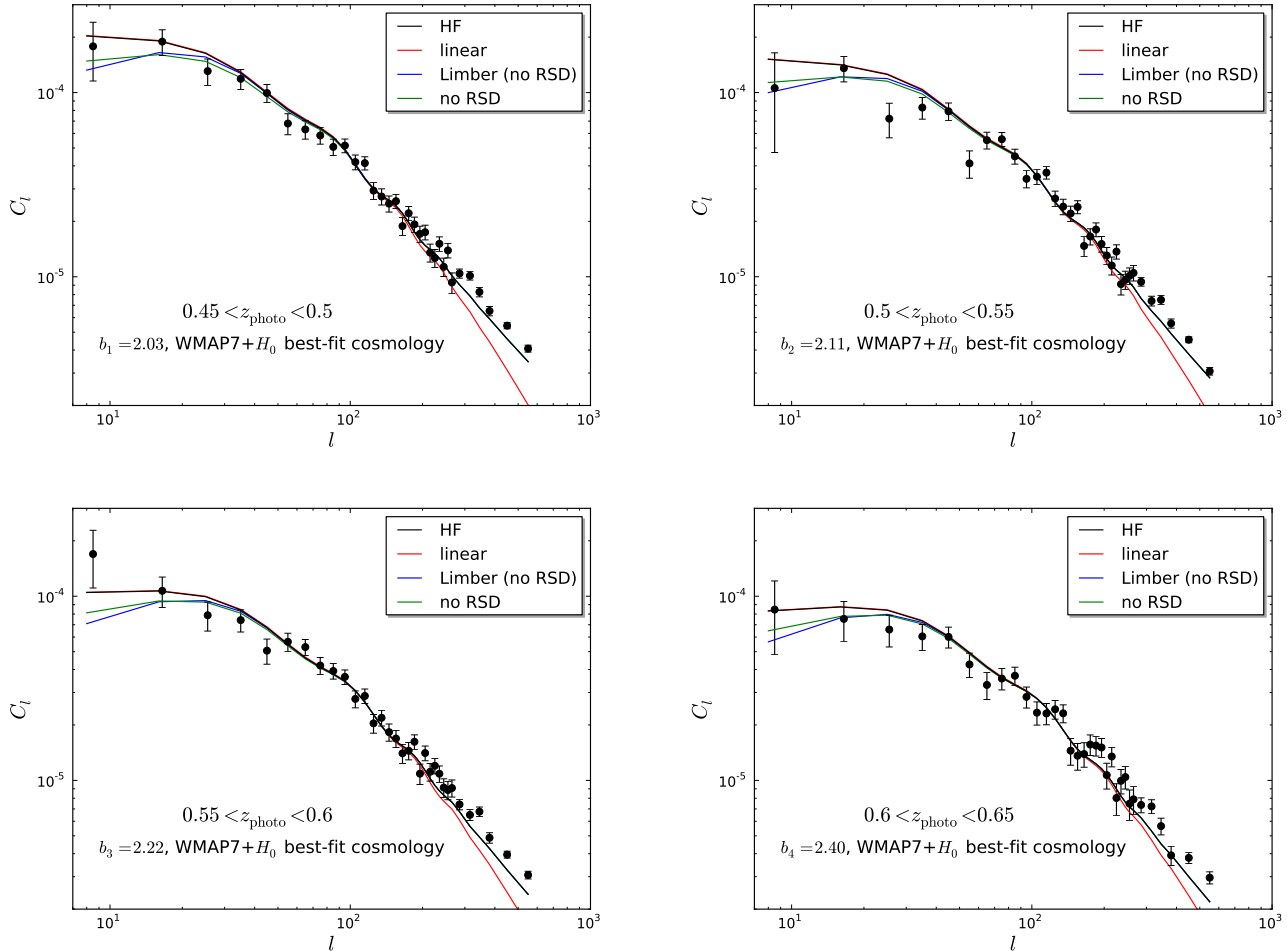


FIG. 2.— Observed power spectra (black points) with error bars and theoretical power spectra (solid curves). We show the theoretical power spectra for different models: the default, HaloFit (HF) based model used in our analysis (black; see text for details), the same model, but using the linear matter power spectrum as input (red), the default model, but using the Limber approximation (blue) and the default model without redshift space distortions (green). We restrict ourselves to the range $\ell = 30 - 200$ in our analysis. For the theoretical spectra, we assume the WMAP7+HST best-fit cosmology and use the bias b_i that best fits the data. We do not here include the shot noise parameters a_i .

unit redshift), $d(z)$ is the comoving distance to redshift z (assuming a flat universe) and \mathbf{v} is the galaxy velocity field. The velocity term arises because gradients of the peculiar velocity contribution to the distance in redshift space change the volume, and consequently, the number density¹⁴.

We assume a linear, scale-independent bias for the galaxy density,

$$\delta_g(\mathbf{x}, z) = b_g(z) \delta_m(\mathbf{x}, z), \quad (6)$$

with δ_m the matter overdensity. For the peculiar velocity field, we use the continuity equation in the linear regime, which gives for a Fourier mode with wave vector \mathbf{k} ,

$$\mathbf{v} = -i\beta(z)\delta_g(\mathbf{k})\frac{\mathbf{k}}{k^2}, \quad (7)$$

¹⁴ Instead of writing the projected galaxy overdensity as an integral over the observed redshift (including peculiar velocity contributions) as in Eq. (4), one could equivalently do the integral over “true” cosmic redshift, see Ref. Padmanabhan et al. (2007), in which case only the true three-dimensional galaxy overdensity appears explicitly and the redshift space distortions come in through a modification of the distribution $g_i(z)$.

where $\beta(z) = f(z)/b_g(z)$ is the redshift distortion parameter and

$$f(z) \equiv \frac{d \ln D(z)}{d \ln a} \quad (8)$$

is the growth factor (with $D(z)$ the linear growth function). In the presence of neutrinos, the growth function is no longer scale independent at late time as the neutrinos suppress growth on scales below the free streaming length Hu & Eisenstein (1998); Eisenstein & Hu (1997), but not on larger scales (with a broad transition regime in between). We shall ignore the scale dependent growth in $\beta(z)$ since it is a small ($\ll 10\%$) correction to the already small effect (on the scales of interest here) of redshift space distortions (RSD, see Fig. 2). However, this scale-dependent growth is included in the real space power spectrum, as this is the main signature of massive neutrinos.

We simplify our treatment of the galaxy bias by following the approach of our two companion papers, adding four free parameters b_i to describe the bias in each bin. The results from our simulations barely change when considering a bias $b_g(z)$ that varies within redshift bins,

showing that this is a safe approximation¹⁵. It then follows from the above (see Fisher et al. (1994); Heavens & Taylor (1995); Padmanabhan et al. (2007)) that

$$C_\ell^{(ii)} = b_i^2 \frac{2}{\pi} \int k^2 dk P_m(k, z=0) \left(\Delta_\ell^{(i)}(k) + \Delta_\ell^{\text{RSD},(i)}(k) \right)^2, \quad (9)$$

where $P_m(k, z=0)$ is the matter power spectrum at redshift zero and

$$\Delta_\ell^{(i)}(k) = \int dz g_i(z) T(k, z) j_\ell(kd(z)). \quad (10)$$

Here, j_ℓ is the spherical Bessel function and $T(k, z)$ the matter transfer function relative to redshift zero¹⁶. The contribution due to redshift space distortions is

$$\Delta_\ell^{\text{RSD},(i)}(k) = \beta_i \int dz g_i(z) T(k, z) \left[\frac{(2l^2 + 2l - 1)}{(2l + 3)(2l - 1)} j_l(kd(z)) - \frac{l(l-1)}{(2l-1)(2l+1)} j_{l-2}(kd(z)) - \frac{(l+1)(l+2)}{(2l+1)(2l+3)} j_{l+2}(kd(z)) \right]. \quad (11)$$

To compute the matter power spectrum at a given redshift $P_m(k, z) = P_m(k, z=0) T^2(k, z)$, we first make use of the CAMB code Lewis et al. (2000), which provides the linear power spectrum by integrating the Boltzmann equations of all species including massive neutrinos. We then apply the HaloFit prescription¹⁷ Smith et al. (2003) to the linear power spectrum to account for non-linear effects on the matter power spectrum.

While in the linear regime the galaxy spectrum is easy to model, calculations on non-linear scales inevitably have large uncertainties. This effect is aggravated by the presence of massive neutrinos since for the massive neutrino case the non-linear regime has been explored less extensively in the literature than for a vanilla Λ CDM model. In the non-linear regime, the matter power spectrum receives corrections due to gravitational collapse, the galaxy bias becomes scale-dependent, and redshift space distortions receive important contributions from velocity dispersion in collapsed objects. We take into account non-linear corrections to the matter spectrum using HaloFit. The effect of non-linearities on redshift space distortions at the relevant scales here is small as it is largely washed out by line-of-sight projection. However, we do expect significant corrections to our model on small scales due to non-linear galaxy bias, which we address below.

For angular scales where non-linear effects cannot be ignored, the contribution to a given angular mode ℓ from a redshift z comes exclusively from three-dimensional modes with wave vector $k \approx \ell/d(z)$. Clearly, to avoid

¹⁵ A similar approach is considered to model $\beta(z)$, appearing in the redshift space distortion contribution. For each bin we calculate an effective growth rate $f_i = (\Omega_{\text{DM}}(z_i))^{0.56}$ where z_i is the mean redshift of the i -th bin, ignoring the scale dependence of the RSD growth.

¹⁶ The transfer function is defined as $\delta_m(\mathbf{k}, z) = T(k, z) \delta_m(\mathbf{k}, z=0)$.

¹⁷ Recently, Bird et al. (2011) developed an extension to HaloFit that incorporates the effect of massive neutrinos. We do not use this prescription as the correction to standard HaloFit is negligible on the scales of our interest.

large non-linear corrections, the analysis must be restricted to low ℓ . On the other hand, the density of modes per unit ℓ increases with ℓ so we want to use as many modes as possible without biasing the results. Figure 3 (left panel) depicts (as a function of redshift z) the value of ℓ above which non-linear corrections to the three-dimensional power spectrum contributions to the angular spectrum become important (i.e. $\ell_{\text{NL}} \equiv k_{\text{NL}}(z) d(z)$), considering various assumptions for the non-linear scale $k_{\text{NL}}(z)$. Given that most of our signal is produced in the range $z = 0.45 - 0.65$, and assuming that our model becomes inadequate at $k > 0.15 h \text{Mpc}^{-1}$, we conclude that a conservative choice would be ℓ_{max} somewhere between 150 and 200.

Alternatively, we can obtain an indication of the importance of non-linear galaxy bias by considering the effect of non-linear corrections to the *matter* power spectrum¹⁸ (which we *do* include in our model). The right panel in Figure 3 therefore shows the signal to noise ratio squared in the difference between our default model and the same model, but using the linear matter power spectrum instead of the non-linear (HaloFit) one. The signal to noise reaches one somewhere between $\ell_{\text{max}} = 150$ and 200, corresponding to contributions of modes $k_{\text{max}} \approx 0.10 h \text{Mpc}^{-1}$ and $k_{\text{max}} \approx 0.14 h \text{Mpc}^{-1}$ at the median redshift $z = 0.55$. Finally, a more concrete indication of the importance of non-linear galaxy bias to the range of scales of our choice is given by Fig. 13 (left panel) of Hamaus et al. (2010), which shows the halo bias as a function of three-dimensional mode k . Since for our sample of galaxies the bias $b \sim 2$, the plot confirms that there is only a mild bias variation in the relevant range of three-dimensional scales relevant to the multipole range we have chosen.

Based on the above discussion, we choose a default value $\ell_{\text{max}} = 200$, but we will also present results for the more conservative choice $\ell_{\text{max}} = 150$. While it is possible to model the galaxy spectrum in a more sophisticated manner (see e.g. Saito et al. (2008, 2009, 2011) for an approach based on perturbation theory and the local bias model McDonald (2006), and Swanson et al. (2010) for a cross-comparison of a number of methods), we consider it appropriate, given the multipole range we include, to use the simple model described in Eq. (9), characterized by bias parameters b_i . In addition to this model, we also consider an alternative model with more freedom, by adding shot noise-like parameters a_i (see also our companion papers),

$$C_\ell^{(ii)} = b_i^2 \frac{2}{\pi} \int k^2 dk P_m(k, z=0) \left(\Delta_\ell^{(i)}(k) + \Delta_\ell^{\text{RSD},(i)}(k) \right)^2 + a_i. \quad (12)$$

The parameters a_i serve to mimic effects of scale-dependent galaxy bias and to model the effect of potential insufficient shot noise subtraction. This model is a version of what is sometimes referred to as the ‘‘P-model’’ (e.g. Hamann et al. (2008); Swanson et al. (2010)) and is independently motivated by the halo model Seljak (2000, 2001); Schulz & White (2006); Guzik et al. (2007) and the local bias ansatz Scherrer & Weinberg (1998); Coles

¹⁸ However, one must keep in mind that this may underestimate the effect of non-linear galaxy bias, as galaxies are more strongly clustered than matter and are thus prone to larger non-linear corrections.

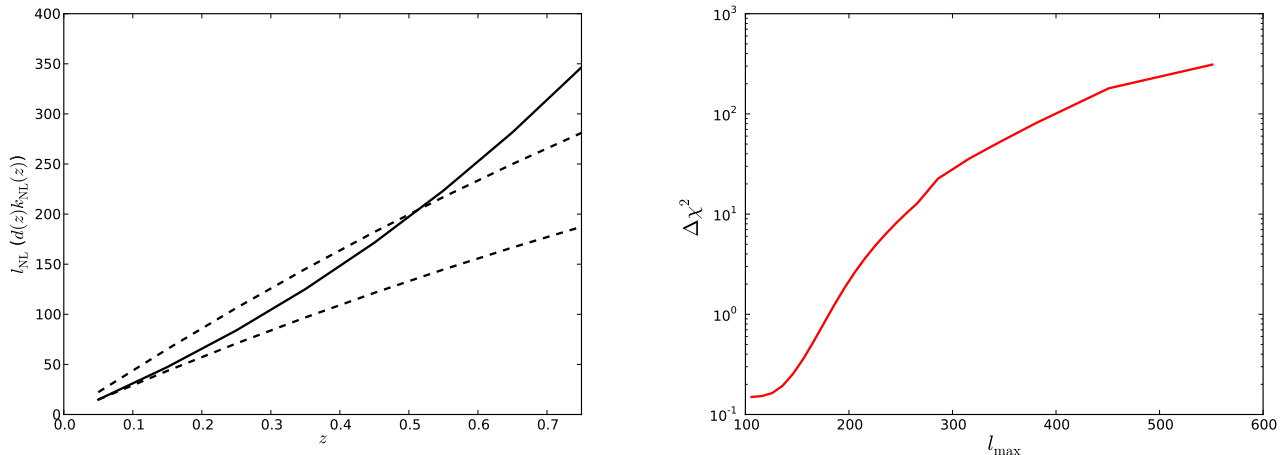


FIG. 3.— *Left panel:* Minimum multipole at which 3-D power spectrum contribution to the angular power spectrum receives important non-linear corrections, as a function of redshift, $l_{\text{NL}} \equiv k_{\text{NL}} d(z)$. We consider several choices of the non-linear scale k_{NL} . The dashed curves are for $k = 0.15 h\text{Mpc}^{-1}$ (top) and $0.1 h\text{Mpc}^{-1}$ (bottom). The solid curve is for a simple model of a redshift dependent $k_{\text{NL}}(z) = R_{\text{NL}}(z = 0)/R_{\text{NL}}(z) \times 0.1 h\text{Mpc}^{-1}$, where $R_{\text{NL}}(z)$ is such that the matter overdensity variance averaged over spheres with this radius equals one (using the linear power spectrum). *Right panel:* The χ^2 difference as a function of l_{max} between our default template, which uses Halofit, and a template using the linear matter power spectrum, given the covariance matrix for the CMASS spectra. We assume the WMAP7 plus HST best fit cosmology and fix the bias parameters $b_i = 2$ ($a_i = 0$). Both plots suggest that non-linear effects start to become (mildly) relevant at l_{max} between 150 and 200.

et al. (1999); Saito et al. (2009). We further discuss the validity of the parameterizations with and without a_i in section 5.

Figure 2 shows the theoretical galaxy spectra as described in this section. The error bars follow from the optimal quadratic estimator method used to construct the power spectra (see Ho et al. (2012) for details). Comparing the spectra with (black) and without (green) redshift space distortions shows that this effect is negligible for $\ell > 50$ and is probably not relevant for the range of scales we use in our data analysis, i.e. $\ell > 30$. Although we never employ it, we also show the effect of using the Limber approximation Limber (1954) and find that for $\ell > 30$ it works excellently.

4. COSMOLOGICAL SIGNATURE OF NEUTRINOS

In the analysis presented in this paper we assume that there are three species of massive neutrinos with equal masses m_ν . Massive neutrinos affect galaxy formation at scales below the Hubble horizon when they become non relativistic,

$$k_{nr} \simeq 0.0145 \left(\frac{m_\nu}{1 \text{ eV}} \right) \sqrt{\Omega_{\text{DM}}} h\text{Mpc}^{-1}, \quad (13)$$

with Ω_{DM} the present total dark matter energy density, i.e. cold dark matter plus massive neutrinos, relative to the critical density. The non-relativistic neutrino overdensities cluster at a given redshift z only at scales where the wavenumber of perturbations is below the neutrino free streaming scale

$$k_{fs}(z) = \frac{0.677}{(1+z)^{1/2}} \left(\frac{m_\nu}{1 \text{ eV}} \right) \sqrt{\Omega_{\text{DM}}} h\text{Mpc}^{-1}, \quad (14)$$

due to the pressure gradient, which prevents gravitational clustering. On spatial scales larger than the free streaming scale $k < k_{fs}$, neutrinos cluster and behave as cold dark matter (and baryons). Perturbations with co-moving wavenumber larger than the free streaming scale

can not grow due to the large neutrino velocity dispersion. As a consequence, the growth rate of density perturbations decreases and the matter power spectrum is suppressed at $k > k_{fs}$. Since the free streaming scale depends on the individual neutrino masses and not on their sum, a measurement of k_{fs} could, in principle, provide the ordering of the neutrino mass spectrum. In practice, such a task appears extremely challenging, see Jimenez et al. (2010).

Figure 4 illustrates the effect of massive neutrinos on the angular power spectra. The solid curves depict the results for the four redshift bins exploited here in the case of a Λ CDM model assuming no massive neutrino species and best fit parameters to WMAP7 year data Larson et al. (2010); Komatsu et al. (2010) and HST- H_0 data Riess et al. (2011). The dashed curves denote the angular power spectra results assuming three massive neutrinos with $\sum m_\nu = 0.3 \text{ eV}$ and keeping the cold dark matter mass energy density constant. In the presence of massive neutrinos the angular power spectra are suppressed at each redshift at an angular scale that is related to the free streaming scale by $\ell \sim d(z) k_{fs}(z)$. Therefore, the larger the neutrino mass (or the redshift), the larger the lowest angular wavenumber at which the power spectrum is maximally suppressed. In the redshift range of interest here and for $\sum m_\nu = 0.3 \text{ eV}$, the suppression angular scale appears in the range $\ell = 20 - 50$ (however, there is some suppression even at lower ℓ). Note as well that there will exist a strong degeneracy between the neutrino masses and the amount of cold dark matter, since, in principle, one could partially compensate the growth suppression induced by massive neutrinos at scales $k > k_{fs}$ by increasing the cold dark matter mass-energy density. Combination with CMB and H_0 data will help to break this degeneracy.

Neutrino masses affect the angular power spectra C_ℓ , see Eq. (9), in two different ways: suppressing galaxy clustering and the growth of structure via $P_m(k)$ as well

as modifying the background expansion rate via the co-moving distance which appears in the argument of the Bessel function j_ℓ . Among these two effects (i.e. growth versus background) we find that the growth suppression effects in the matter power spectrum due to the presence of massive neutrinos will dominate over background effects. Therefore, the neutrino mass constraints presented in the following analysis arise mostly from the suppression of clustering rather than from purely geometrical effects.

5. MOCKS

We first consider angular spectra based on mock galaxy catalogs to test that neither our method of estimating the spectra nor our modeling of the spectra introduces a bias in the reconstructed cosmological parameters. We use twenty independent CMASS mock catalogs based on N-body simulations and a Halo Occupation Distribution (HOD) model described in White et al. (2011) (see also our companion papers Ho et al. (2012); Seo et al. (2012) for details). The input cosmology for the simulations is $\Omega_{\text{DM}} = 0.274, h = 0.7, \Omega_b = 0.046, n_s = 0.95, \sigma_8 = 0.8$ in a spatially flat universe, with n_s and σ_8 the scalar spectral index and the linear rms density fluctuations in spheres of radius $8 h^{-1} \text{Mpc}$ at $z = 0$, respectively. Neutrinos are massless in the input cosmology. The catalogs cover a cubic volume with side $1.5 h^{-1} \text{Gpc}$. To construct an “observed” catalog, we put the observer in one corner of the box and consider the subsample of galaxies in the shell octant between the observer’s $z = 0.5 - 0.55$. For simplicity, we do not apply photometric redshift errors nor do we introduce redshift shifts due to peculiar velocities. This latter effect would only be significant on very large scales anyway (see Figure 2). Each mock covers $\pi/2 \text{ rad}^2$ and consists of about 125,000 galaxies. Since both area and galaxy number are thus roughly half the values for the $z = 0.5 - 0.55$ redshift bin of the true data, the number density is comparable to that of the true photometric sample. We apply this procedure for eight different corners to get eight different lines of sight per simulation. Note, however, that these lines of sight are not completely independent as they are based on the same simulation volume. Finally, for each line of sight, we average the spectra over all twenty independent realizations in order to increase the signal to noise ratio. The covariance matrix for the mock angular power spectrum is rescaled accordingly to reflect the decrease in covariance due to taking the average.

As described in section 3, we consider a model characterized by the cosmological parameters and a galaxy bias b_0 (giving our mock bin the label 0), and a more conservative model with bias b_0 and nuisance parameter a_0 , so that the spectrum is given by

$$C_\ell^{(00)} = b_0^2 \frac{2}{\pi} \int k^2 dk P_m(k, z=0) \left(\Delta_\ell^{(i)}(k) \right)^2 + a_0. \quad (15)$$

In the galaxy bias-only version, a_0 is simply set to zero.

As a direct test of this model, we fit it to the averaged mock spectrum. In this first approach, we keep the cosmology fixed to the mock’s input cosmology and restrict the fit to the range $\ell = 30 - 200$. The only free parameters are thus either b_0 or (b_0, a_0) . We use a modification of the publicly available COSMOMC package

Lewis & Bridle (2002) to sample this parameter space using Monte Carlo Markov Chains (MCMC). We show the resulting best-fit spectra together with the mock average in Fig. 5. Considering first the default, galaxy bias-only model (black curve), we find that the best fit to the mock result has a linear bias $b_0 = 2.02$ (with uncertainty $\sigma(b_0) < 0.01$) and has $\chi^2 = 11.3$. This should be compared to an expectation value of $\langle \chi^2 \rangle = 16$ based on 17 data bins and one free parameter. The galaxy bias model thus provides a good fit to the simulated spectrum (the probability of getting a χ^2 lower than 11.3 for an expectation value of 16 is approximately 20%).

Next, including the shot noise-like parameter a_0 to take into account potential residual shot noise and/or non-linear effects not captured by our simple Halofit plus scale-independent galaxy bias model, we find a best fit model with $a_0 = 1.1 \cdot 10^{-6}$ and $b_0 = 2.00$. However, the uncertainty in a_0 is $\sigma(a_0) = 1.0 \cdot 10^{-6}$ so the preference for a non-zero value cannot be considered significant. In this model, we find $\chi^2 = 10.1$, to be compared to the expected $\langle \chi^2 \rangle = 15$. This is only a marginal ($\Delta\chi^2 \approx 1.2$) improvement.

Restricting the fitting range to $\ell = 30 - 150$, we find $\Delta\chi^2 = 1.1$ between the two best-fit models, and $a_0 = (1.8 \pm 1.9) \times 10^{-6}$.

The comparison above suggests that for the range $\ell = 30 - 200$, the galaxy bias model without an extra nuisance parameter may be sufficient. We now undertake a more complete check of our model and the entire cosmology analysis by using MCMC to fit the full space of cosmological parameters as well as the galaxy bias (and shot noise parameter) to the averaged mock spectrum. The differences between the resulting best-fit parameter values and the “true”, i.e. input, values give an indication of the parameter bias introduced by our method. To break parameter degeneracies, while not letting the prior bias us away from the input cosmology, we include a “mock” CMB prior¹⁹, which will provide a likelihood similar to the true WMAP7 one, except shifted to be centered around the mock input parameters.

We want any deviation between the input cosmology and the recovered cosmology to be small compared to the uncertainty level of the actual data. We therefore take information from our final results and use the uncertainties for the WMAP+HST+CMASS ($\ell_{\text{max}} = 200$) real data case for comparison. If the biases on parameter estimation are small compared to these numbers, it provides strong motivation for considering our approach sound, as most uncertainties in the next section will be larger than in the WMAP+HST+CMASS case. Therefore, parameter uncertainties σ referred to in the remainder of this section are these data-based uncertainties.

Starting with the parameter space²⁰ $\{\Omega_b h^2, \Omega_{\text{DM}} h^2, \theta, A_s, n_s, \tau, b_0\}$, we find that all cosmological parameters are reproduced to within 1σ of

¹⁹ The “mock” CMB prior is defined by $\chi_{\text{WMAP7}}^2 \equiv (p_i - p_{i,\text{input}}) \text{COV}_{ij}^{-1} (p_j - p_{j,\text{input}})$, where p_i are the parameters at each point of the chain, $p_{i,\text{input}}$ the input parameters, COV_{ij} is the WMAP7 covariance matrix and i, j are summed over.

²⁰ The parameters θ, A_s and τ represent the ratio between the sound horizon and the angular diameter distance at decoupling, the scalar amplitude of primordial fluctuations and the reionization optical depth, respectively.

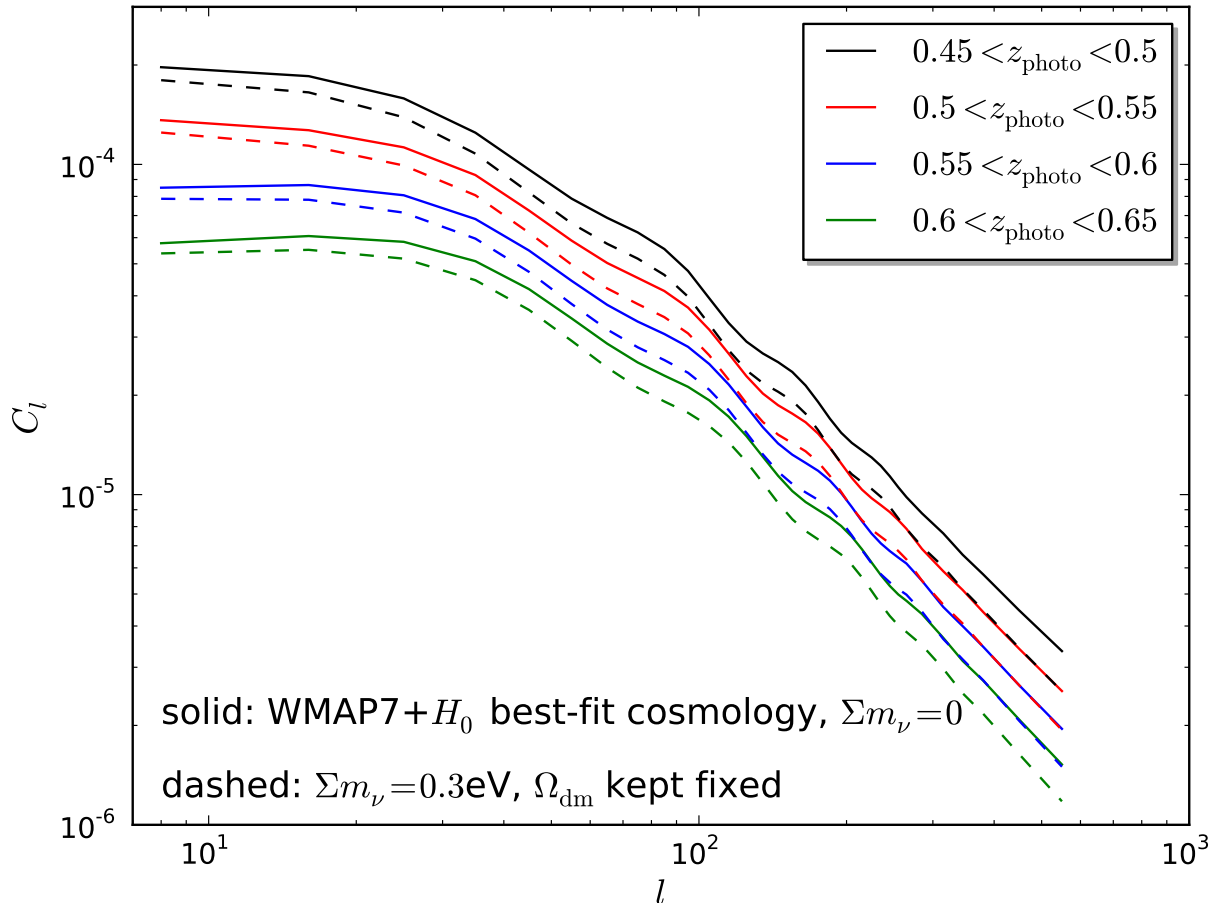


FIG. 4.— Effect of neutrinos on the angular power spectra. The solid and dashed curves depict the massless and $\Sigma m_\nu = 0.3$ eV cases, respectively.

the input values (although the parameter most affected by the mock CMASS data, $\Omega_{\text{DM}}h^2$, is higher than the input by close to 1σ).

Unfortunately, we do not have mocks based on a cosmology with non-zero Σm_ν . One check we *can* do, however, is to fit a model with parameters $\{\Omega_b h^2, \Omega_{\text{DM}} h^2, \theta, A_s, n_s, \tau, \Sigma m_\nu, b_0\}$ to our $\Sigma m_\nu = 0$ mock spectra. The parameters affected by far the most by the angular spectra are (again) $\Omega_{\text{DM}} h^2$ and Σm_ν . We show the posteriors of this calculation in Fig. 6. In the left panel, the vertical lines indicate the $\Omega_{\text{DM}} h^2$ input value, and the 1σ and 2σ bounds based on the uncertainty σ from the actual data. The blue points with error bars are the posterior mean values and 1σ recovered errors after fitting to the averaged mock spectrum. Note that the recovered error bars (from the averaged mock power spectrum) are typically similar to the data-based error bars. While the different lines of sight are not entirely independent, Fig. 6 points towards a bias of about $1 - 1.5\sigma$ in $\Omega_{\text{DM}} h^2$. For the neutrino mass, the right panel shows the posterior probability distributions in blue. The posteriors are always consistent with the input value $\Sigma m_\nu = 0$ and can be interpreted as providing upper bounds. We have made the same plot as in the left panel for the other parameters and they were biased

significantly less (as their reconstruction is dominated by the mock CMB prior).

Adding the nuisance parameter a_0 , we obtain the red points and curves in Fig. 6. The effect of marginalizing over a_0 is to diminish the parameter bias so that $\Omega_{\text{DM}} h^2$ is typically reconstructed to well within 1σ . We attribute this change to a_0 accounting for a possible scale-dependence in galaxy bias on quasilinear scales. The neutrino constraints are also still consistent with the input, although the mock upper limits do become significantly weaker. We have also studied mock cosmology constraints using $\ell_{\text{max}} = 150$, and found that the main effect is to widen the posterior distributions slightly, while the change in parameter bias relative to $\ell_{\text{max}} = 200$ is small.

We conclude that our galaxy bias-only model and the fitting method used here properly reproduce the input cosmology for our choices of ℓ_{max} , except that there is a bias of about $1 - 1.5\sigma$ in $\Omega_{\text{DM}} h^2$. The model with nuisance parameter a_0 removes this parameter bias at the cost of larger error bars. While the bias in $\Omega_{\text{DM}} h^2$ is not extreme, being only slightly above the 1σ level, it is sufficiently worrying that we will quote results for the galaxy bias-only model *and* for the more conservative model with shot noise-like parameters. Changing ℓ_{max}

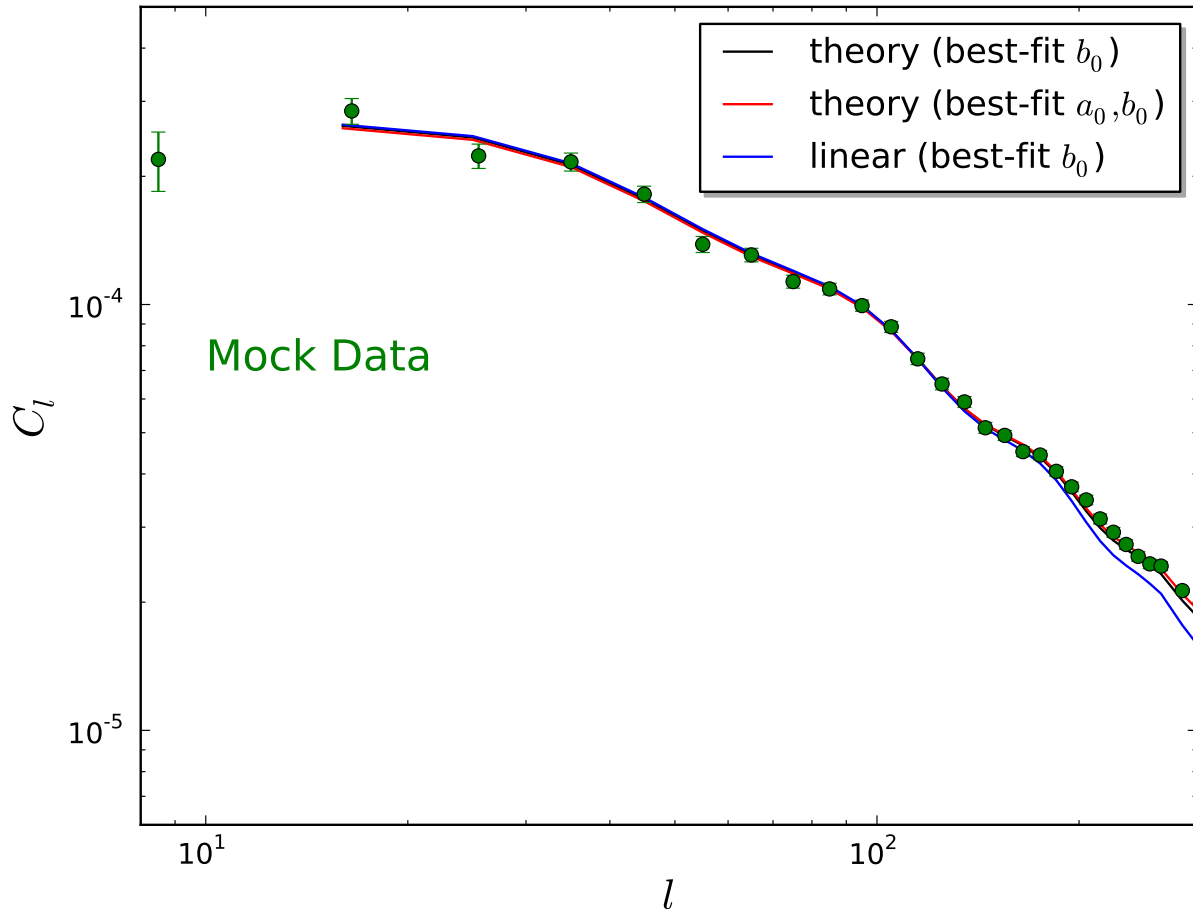


FIG. 5.— Example of an averaged mock spectrum (green points with error bars) and theoretical spectra (solid lines). Fixing the cosmology to the mock input cosmology (see text), we fit the averaged mock spectrum in the range $\ell = 30 - 200$ to our model described in the text. The black curve is the resulting best-fit spectrum if we only fit a (scale-independent) galaxy bias b_0 (best-fit value $b_0 = 2.02$), while the red curve is the best fit in a model that also includes the nuisance parameter a_0 (best fit values $b_0 = 2.00$, $a_0 = 1.05 \cdot 10^{-6}$). To provide a hint of the importance of non-linear effects in this multipole range, we plot the spectrum based on a linear three dimensional matter power spectrum in blue ($b_0 = 2.02$, $a_0 = 0$)

between 150 and 200 does not have a large effect on how well the models compare to mocks, suggesting that both are reasonable choices. We will quote results for both ranges.

6. RESULTS

While the CMASS angular galaxy power spectra carry useful information about the sum of neutrino masses Σm_ν , the effect of Σm_ν is degenerate with certain other parameters which are not well constrained from the angular spectra alone. There are many combinations of external data sets that our angular spectra can be combined with to fix this problem. One approach would be to optimize the neutrino bound by combining as many data sets as possible. However, we choose instead to focus as much as possible on the effect of the CMASS photometric data and therefore consider mostly simple priors. Our two main prior choices are WMAP7 CMB data Larson et al. (2010) and the combination of WMAP7 with the HST measurement of the Hubble parameter Riess et al. (2011). At the end of this section, we will briefly consider the effect of adding the Union 2 supernova com-

pilation Amanullah *et al* (2010) and the measurement of the BAO scale based on SDSS Data Release 7 Abazajian et al. (2009) spectroscopic data from Ref. Percival et al. (2010).

We again use a modification of the publicly available COSMOMC package Lewis & Bridle (2002) to sample the parameter space using MCMC. Our parameter space consists of the six usual Λ CDM parameters, $(\Omega_b h^2, \Omega_{\text{DM}} h^2, \theta, \ln(10^{10} A_s), n_s, \tau)$, the neutrino mass fraction f_ν , defined as $\Omega_\nu / \Omega_{\text{DM}}$ (where Ω_{DM} includes cold dark matter and massive neutrinos), in addition to A_{SZ} , describing the amplitude relative to a template of the Sunyaev-Zel'dovich contribution to the CMB Komatsu & Seljak (2002), the four galaxy bias parameters b_i and (optionally) the four nuisance parameters a_i , leaving us with a maximum total number of parameters of sixteen parameters. We put uniform priors on these parameters and derive Σm_ν using Eq. (1).

We first consider the WMAP7 prior and show how the neutrino bound improves as CMASS data are added. The resulting 95% CL upper limits are shown in the top

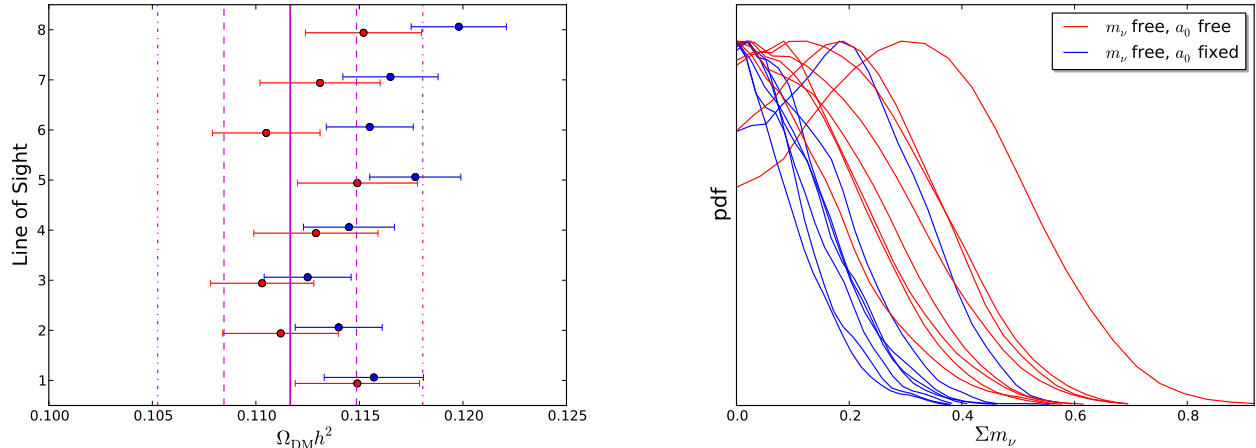


FIG. 6.— *Left panel:* Recovered values of $\Omega_{\text{DM}} h^2$ from averaged mock spectrum together with CMB prior. We consider spectra from eight different lines of sight. The points with error bars show the posterior mean values and 1σ error bars after the Monte Carlo analysis for two scenarios: varying Σm_ν with (red) and without (blue) a_0 marginalized. The vertical magenta lines indicate the input value $\Omega_{\text{DM}} h^2 = 0.11166$ (solid) and the input \pm one and two σ , where $\sigma = 0.0032$ is the parameter uncertainty based on the data set WMAP7+HST+angular spectra ($a_i = 0$ fixed). There is a bias of about 1σ without the nuisance parameter, which disappears when a_i is marginalized over. *Right panel:* The posterior neutrino mass distributions for the two cases discussed above. The mock constraints are consistent with the input cosmology of $\Sigma m_\nu = 0$. Other parameters are all reconstructed to close to their input values and are not strongly affected by the angular spectra.

95% CL Σm_ν [eV]	prior only	prior+CMSS, $\ell_{\text{max}} = 150$	prior+CMSS, $\ell_{\text{max}} = 200$
WMAP7 prior	1.1	0.74 (0.92)	0.56 (0.90)
WMAP7 + HST prior	0.44	0.31 (0.40)	0.26 (0.36)

TABLE 1

THE 95% CONFIDENCE LEVEL UPPER LIMITS ON THE SUM OF THE NEUTRINO MASSES Σm_ν . THE TOP ROW INVESTIGATES THE EFFECT OF ADDING THE CMSS GALAXY POWER SPECTRA TO A WMAP PRIOR WHILE THE BOTTOM ROW USES WMAP AND THE H_0 CONSTRAINT FROM HST AS A PRIOR. IN PARENTHESES WE SHOW RESULTS FOR THE MORE CONSERVATIVE MODEL MARGINALIZING OVER THE SHOT NOISE-LIKE PARAMETERS a_i .

row of Table 1, with the results with a_i marginalized in parentheses. The bound improves from 1.1 eV for CMB only to 0.56 eV for CMB with CMSS data ($\ell_{\text{max}} = 200$). This constraint is comparable to the limit $\Sigma m_\nu < 0.62$ eV derived by Reid et al. (2010) from the DR7 spectroscopic sample. It thus appears that the advantage of spectroscopic redshifts (providing information on clustering along the line of sight) in that sample is offset by the advantage of the current sample having a larger volume, although there are other differences between the samples and analyses as well. Note, however, that the constraint deteriorates significantly when marginalizing over the nuisance parameters a_i . In this case, the mass bound is not significantly better than with CMB alone. We show the posterior probability distributions for Σm_ν and the other cosmological parameters in Fig. 7.

We next consider the constraints using WMAP7 with HST H_0 prior. The CMB alone provides a strong measurement of one combination of late-universe parameters through its sensitivity to the distance to the last scattering surface. However, this distance measurement leaves a degeneracy between Ω_Λ and Σm_ν , so that the CMB-only limit on the neutrino mass arises mainly from the effect of neutrinos on the primary anisotropies and not from this distance measurement. Measuring H_0 constrains a different combination of late universe parameters and thus breaks the CMB degeneracy. This is why

the WMAP7+HST bound is so much stronger than the WMAP7-only one, i.e. $\Sigma m_\nu < 0.44$ eV as opposed to $\Sigma m_\nu < 1.1$ eV. Adding the CMSS angular spectra tightens the bound significantly so that an impressive upper bound of $\Sigma m_\nu < 0.26$ eV is reached for $\ell_{\text{max}} = 200$ (in the bias-only model), as is shown in the second row of Table 1. The effect of marginalization over a_i is again to bring the constraint back closer to the CMB+HST bound.

The posteriors for all cosmological parameters are shown in Fig. 8. In addition to the full likelihoods for Σm_ν , summarized in Table 1, the $\Omega_{\text{DM}} h^2$ posteriors are worth noting. The effect of the angular spectra is to strongly shift the average value of this parameter (blue curve), while including the nuisance parameters (red curve) weakens the shift. The last two parameters in Fig. 8 (and 7), Ω_Λ and H_0 , are not independent and can be expressed in terms of the preceding parameters. The shift thus is really only significant for one independent parameter, $\Omega_{\text{DM}} h^2$, in our basis. The results in section 5 suggest that the shift in the bias-only case might partially be a bias due to our model and that the results with a_i marginalized are unbiased.

We do not explicitly show the correlations between parameters, but have verified that, in the CMB+CMSS case, the neutrino mass has its strongest degeneracies with $\Omega_{\text{DM}} h^2$, the bias parameters b_i and σ_8 . While, in

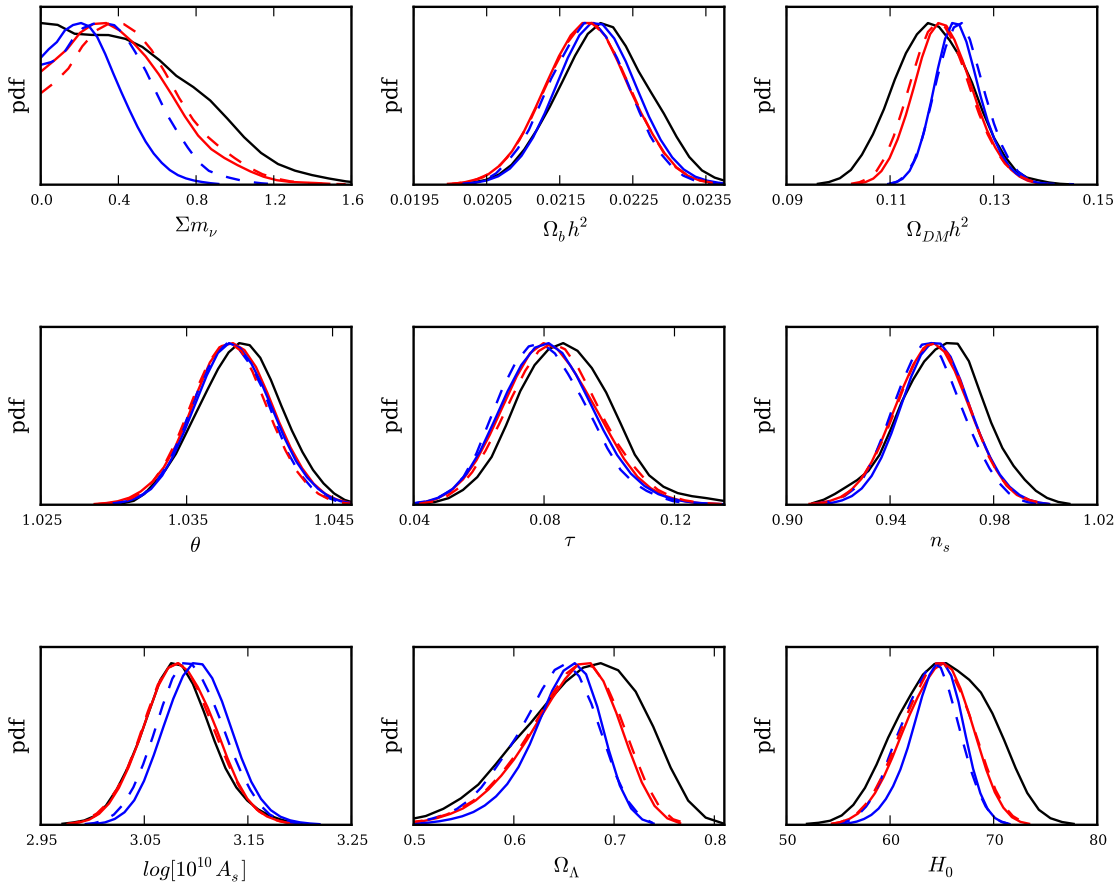


FIG. 7.— Cosmological constraints with a WMAP7 CMB prior. We show the probability distribution functions for CMB only (black), CMB with CMASS spectra in the range $\ell = 30 - 150$ (blue dashed) and CMB with CMASS spectra in the range $\ell = 30 - 200$ (blue solid). The red curves represent the constraints in the conservative model where we marginalize over a set of nuisance parameters a_i .

agreement with our discussion in section 4, the inclusion of the Hubble prior removes the $\Sigma m_\nu - \Omega_{\text{DM}} h^2$ degeneracy, the strong correlations with b_i and σ_8 remain.

We have also added supernova and BAO data to the CMB+HST+CMASS data set, and considered the neutrino mass bound in the bias-only model, but we found negligible improvement (from 0.26 eV to 0.25 eV) relative to the case without these additional data sets. These additional data sets do carry significant information, but this information is degenerate with the information already present in the three default data sets.

For the multipole range $\ell = 30 - 150$, we show the results using dashed lines in Figures 7 and 8. The 95% CL upper limit for CMB+HST+CMASS in this case is 0.31(0.40) eV and for CMB+CMASS it is 0.74(0.92) eV fixing (varying) $a_i = 0$. A significant amount of information is thus contained in the large ℓ range of multipoles, which makes sense as the number of modes is large.

Finally, we consider the question of where most of the neutrino mass information comes from. In principle, massive neutrinos affect the angular power spectra both by their small-scale suppression of the three-dimensional power spectrum, and by changing the projection of physical scales onto angular scales through their effect on the

background expansion. As discussed in section 4, we expect the former effect to carry more constraining power than the latter effect. We test this by running Monte Carlo chains where the effect of massive neutrinos on the three-dimensional power spectrum is artificially taken out, while the effect on the background expansion is left intact. Specifically, we replace the usual linear CAMB power spectrum by the spectrum given by the Eisenstein and Hu (EH) fitting formula Eisenstein & Hu (1998), which does not include the effect of massive neutrinos. We find that in this setup, including the CMASS galaxy power spectra does *not* improve the neutrino mass bound relative to the case with CMB, or with CMB+HST, only. In other words, the projection effect alone carries little information on neutrino mass (at least after marginalizing over the effects of other parameters) and the bounds quoted in this manuscript can be attributed to the small-scale suppression of the three-dimensional power spectrum.

7. CONCLUSIONS

We have exploited angular power spectra from the SDSS-III DR8 sample of photometric galaxies with CMASS selection criteria to put interesting constraints

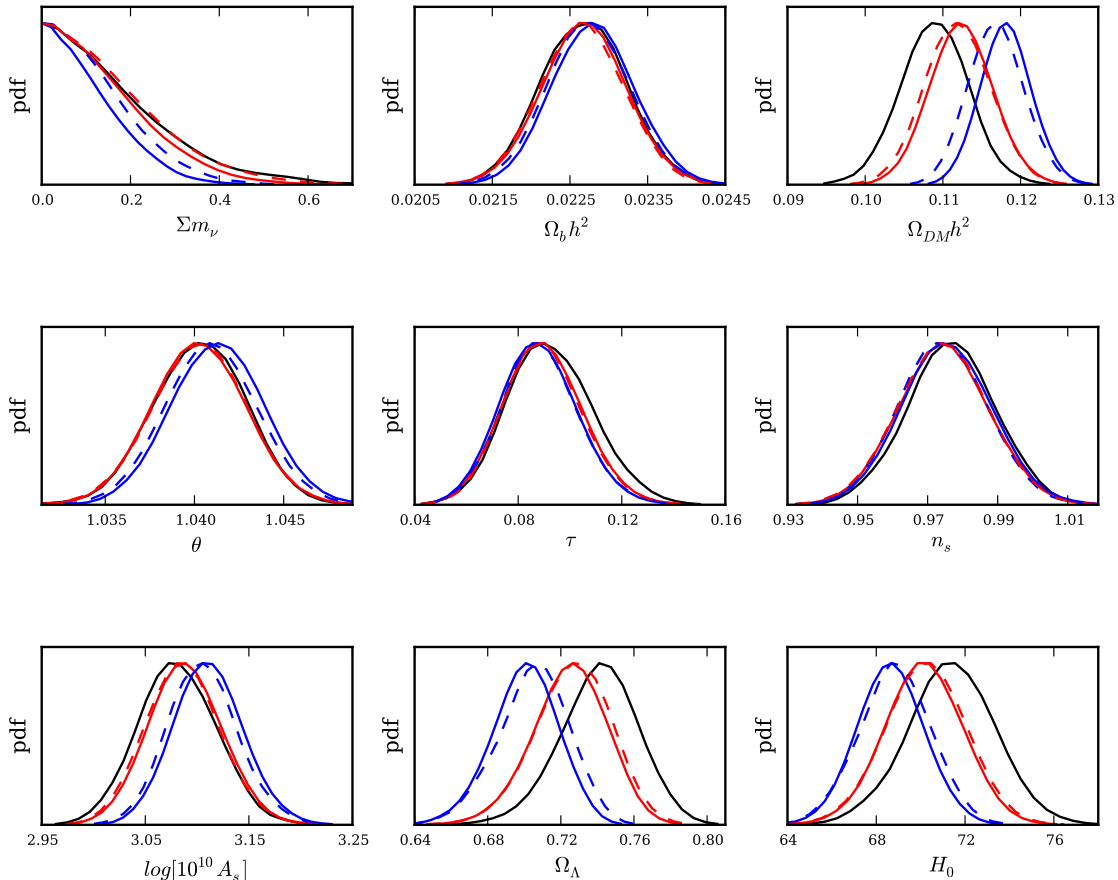


FIG. 8.— Cosmological constraints with a WMAP7 CMB *and* Hubble parameter prior. We show the probability distribution functions for CMB + H_0 only (black), CMB + H_0 with CMASS spectra in the range $\ell = 30 - 150$ (blue dashed) and CMB + H_0 with CMASS spectra in the range $\ell = 30 - 200$ (blue solid). The red curves represent the constraints in the conservative model where we marginalize over a set of nuisance parameters a_i . While this marginalization degrades the neutrino bound, simulations have shown it removes the bias in $\Omega_{DM}h^2$ (see section 5).

on the sum of neutrino masses. We have used mock galaxy catalogs based on N-body simulations and HOD modeling to test two models for the angular galaxy spectra. Based on these tests, we decided to compare the data to theoretical spectra based on the non-linear matter power spectrum augmented by a linear galaxy bias factor. However, since this model does result in a bias in $\Omega_{DM}h^2$ of $\sim 1 - 1.5\sigma$, we have also fitted the data to a more conservative model, with an additional set of shot noise-like fitting parameters, in which this bias is virtually absent. The tests also motivated us to use the multipole range $\ell = 30 - 200$, but we quoted results for the more conservative choice $\ell = 30 - 150$ as well. The added advantage is that this analysis provides insight into the range of scales that yields the galaxy clustering information.

Combining the CMASS data with a CMB prior from the WMAP7 survey, we find an upper bound $\Sigma m_\nu < 0.56$ eV (0.90 eV) at 95% confidence level for $\ell_{\max} = 200$ in the model with free parameters b_i (b_i and a_i). Adding the HST measurement of the Hubble parameter, the probability distribution tightens and we find $\Sigma m_\nu < 0.26$ eV

(0.36 eV). We have also considered the effect of adding supernova and a (lower redshift) BAO measurement, but when the HST prior is included already, these additions lower the upper limit to 0.25 eV (in the bias-only model). Considering the dependence on the multipole range, characterized by a maximum multipole ℓ_{\max} , we find that a significant amount of information resides in the largest multipoles $\ell = 150 - 200$, but that even for $\ell_{\max} = 150$, the galaxy spectra place a strong bound on neutrino mass. Our main results are summarized in Table 1.

It is interesting to compare these results to the outcome of an analysis of a similar (but smaller) high redshift SDSS photometric catalog, the MegaZ sample Collister et al. (2007). In Thomas et al. (2010), the strongest bound quoted is a 95% CL upper limit of 0.28 eV, including SN and BAO data in addition to CMB, HST and MegaZ. However, this particular bound is based on a multipole range with $\ell_{\max} = 300$ and no nuisance parameters a_i . As we have discussed extensively, we believe $\ell_{\max} = 200$ (or even slightly lower) is a better choice if one wants to avoid significant, unknown non-linear cor-

rections to the galaxy bias. For this choice, the MegaZ sample yields an upper bound of 0.34 eV. Assuming the aggressive, bias-only model (as in the MegaZ analysis), the value we find for the CMASS sample is 0.25 eV, which is thus a significant improvement. However, it must be kept in mind that this model causes a small parameter bias and that the more conservative model yields a weaker bound of 0.36 eV.

The bounds presented here rule out the quasi-degenerate neutrino mass hierarchy. For example, for $\Sigma m_\nu = 0.25$ eV, it follows from $|\Delta m_{23}^2| = 2.5 \cdot 10^{-3}$ eV² that the mass difference $|m_3 - m_2| \approx 0.015$ eV, so that the largest mass difference is $|m_3 - m_2|/(\Sigma m_\nu/3) \approx 20\%$ of the average neutrino mass. We are thus entering the regime where the mass splittings are significant. Looking forward, the prospects are exciting. As the sensitivity of cosmological neutrino mass measurements improves, the sum of the masses will either be measured, i.e. a value that can be distinguished from zero will be found, or the upper limit will be sharpened. However, even in the latter case, interesting things can be learned. If the sum of the masses is found to be less than ~ 0.1 eV, this rules out the inverted hierarchy, leaving the normal hierarchy as the only option. Moreover, even in the normal hierarchy, Σm_ν is not allowed to be lower than ~ 0.05 eV so that sooner or later a measurement, rather than an upper bound, can be expected.

Finally, we note that BOSS is currently taking spectra for a sample of galaxies with the same selection criteria as the galaxies considered in this paper and will reach a sample of approximately 1,500,000 galaxies when finished in 2014. The results presented here and in our companion papers are thus only the tip of the iceberg of what can be done with BOSS. The spectroscopic data

will allow a measurement of the three-dimensional power spectrum for an even larger volume than considered here (if the low redshifts sample is included) so that also clustering in the line-of-sight direction can be resolved, thus promising significantly stronger cosmology constraints than from the photometric data.

Acknowledgement:

Funding for SDSS-III has been provided by the Alfred P. Sloan Foundation, the Participating Institutions, the National Science Foundation, and the U.S. Department of Energy Office of Science. The SDSS-III web site is <http://www.sdss3.org/>.

SDSS-III is managed by the Astrophysical Research Consortium for the Participating Institutions of the SDSS-III Collaboration including the University of Arizona, the Brazilian Participation Group, Brookhaven National Laboratory, University of Cambridge, University of Florida, the French Participation Group, the German Participation Group, the Instituto de Astrofísica de Canarias, the Michigan State/Notre Dame/JINA Participation Group, Johns Hopkins University, Lawrence Berkeley National Laboratory, Max Planck Institute for Astrophysics, New Mexico State University, New York University, Ohio State University, Pennsylvania State University, University of Portsmouth, Princeton University, the Spanish Participation Group, University of Tokyo, University of Utah, Vanderbilt University, University of Virginia, University of Washington, and Yale University.

RdP is supported by FP7-IDEAS-Phys.LSS 240117. O.M. is supported by AYA2008-03531 and the Consolider Ingenio project CSD2007-00060.

REFERENCES

- Abazajian, K. N., Adelman-McCarthy, J. K., Agüeros, M. A., et al. 2009, *ApJS*, 182, 543
- Aihara, H., Allende Prieto, C., An, D., et al. 2011, *ApJS*, 193, 29
- Allen, S., Schmidt, R., & Bridle, S. 2003, *Mon.Not.Roy.Astron.Soc.*, 346, 593
- Amanullah et al. R. 2010, *Astrophys.J.* accepted
- Barger, V., Marfatia, D., & Tregre, A. 2004, *Phys.Lett.*, B595, 55
- Benson, B. A., de Haan, T., Dudley, J. P., et al. 2011, *ArXiv e-prints*
- Bird, S., Viel, M., & Haehnelt, M. G. 2011, *ArXiv e-prints*
- Coles, P., Melott, A. L., & Munshi, D. 1999, *ApJ*, 521, L5
- Collister, A., Lahav, O., Blake, C., et al. 2007, *MNRAS*, 375, 68
- Crotty, P., Lesgourgues, J., & Pastor, S. 2004, *Phys.Rev.*, D69, 123007
- Eisenstein, D. J., & Hu, W. 1997, *Astrophys.J.*, 511, 5
- Eisenstein, D. J., & Hu, W. 1998, *ApJ*, 496, 605
- Eisenstein, D. J., Weinberg, D. H., Agol, E., et al. 2011, *ApJ*, 142, 72
- Eitel, K. 2005, *Nucl.Phys.Proc.Suppl.*, 143, 197
- Elgaroy, O., & Lahav, O. 2005, *New J.Phys.*, 7, 61
- Elgaroy, O., Lahav, O., Percival, W., et al. 2002, *Phys.Rev.Lett.*, 89, 061301
- Fisher, K. B., Scharf, C. A., & Lahav, O. 1994, *MNRAS*, 266, 219
- Fogli, G., Lisi, E., Marrone, A., et al. 2008, *Phys.Rev.*, D78, 033010
- Fogli, G., Lisi, E., Marrone, A., Palazzo, A., & Rotunno, A. 2011
- Fukugita, M., Ichikawa, T., Gunn, J. E., et al. 1996, *AJ*, 111, 1748
- Gomez-Cadenas, J., Martin-Albo, J., Mezzetto, M., Monrabal, F., & Sorel, M. 2011, * Temporary entry *
- Gonzalez-Garcia, M., & Maltoni, M. 2008, *Phys.Rept.*, 460, 1
- Goobar, A., Hannestad, S., Mortsell, E., & Tu, H. 2006, *JCAP*, 0606, 019
- Gunn, J. E., Carr, M., Rockosi, C., et al. 1998, *AJ*, 116, 3040
- Gunn, J. E., Siegmund, W. A., Mannery, E. J., et al. 2006, *AJ*, 131, 2332
- Guzik, J., Bernstein, G., & Smith, R. E. 2007, *MNRAS*, 375, 1329
- Hamann, J., Hannestad, S., Melchiorri, A., & Wong, Y. Y. 2008, *J. Cosmology Astropart. Phys.*, 7, 17
- Hamaus, N., Seljak, U., Desjacques, V., Smith, R. E., & Baldauf, T. 2010, *Phys. Rev. D*, 82, 043515
- Hannestad, S. 2003, *JCAP*, 0305, 004
- . 2005, *Phys.Rev.Lett.*, 95, 221301
- Hannestad, S., & Raffelt, G. 2004, *JCAP*, 0404, 008
- Heavens, A. F., & Taylor, A. N. 1995, *MNRAS*, 275, 483
- Ho, S., Cuesta, A., & Seo, H.-J. et al. 2012, submitted to *ApJ*
- Hu, W., & Eisenstein, D. J. 1998, *Astrophys.J.*, 498, 497
- Jimenez, R., Kitching, T., Pena-Garay, C., & Verde, L. 2010, *JCAP*, 1005, 035
- Komatsu, E., & Seljak, U. 2002, *MNRAS*, 336, 1256
- Komatsu, E., et al. 2009, *Astrophys.J.Suppl.*, 180, 330
- Komatsu, E., Smith, K. M., Dunkley, J., et al. 2010
- Komatsu, E., et al. 2011, *Astrophys.J.Suppl.*, 192, 18
- Larson, D., Dunkley, J., Hinshaw, G., et al. 2010, *ArXiv e-prints*
- Lesgourgues, J., & Pastor, S. 2006, *Phys.Rept.*, 429, 307
- Lewis, A., & Bridle, S. 2002, *Phys.Rev.D*
- Lewis, A., Challinor, A., & Lasenby, A. 2000, *Astrophys.J.*
- Limber, D. N. 1954, *ApJ*, 119, 655
- Lobashev, V. 2003, *Nucl.Phys.*, A719, 153
- McDonald, P. 2006, *Phys. Rev. D*, 74, 103512
- Otten, E., & Weinheimer, C. 2008, *Rept.Prog.Phys.*, 71, 086201
- Padmanabhan, N., Seljak, U., & Pen, U. L. 2003, *New Astronomy*, 8, 581
- Padmanabhan, N., Schlegel, D. J., Seljak, U., et al. 2007, *MNRAS*, 378, 852
- Percival, W. J., Reid, B. A., Eisenstein, D. J., et al. 2010, *MNRAS*

- Pier, J. R., Munn, J. A., Hindsley, R. B., et al. 2003, *AJ*, 125, 1559
- Reid, B. A., Percival, W. J., Eisenstein, D. J., et al. 2010, *Mon.Not.Roy.Astron.Soc.*, 404, 60, * Brief entry *
- Reid, B. A., Verde, L., Jimenez, R., & Mena, O. 2010a, *J. Cosmology Astropart. Phys.*, 1, 3
- . 2010b, 1, 3
- Riemer-Sørensen, S., Blake, C., Parkinson, D., et al. 2011, *ArXiv e-prints*
- Riess, A. G., Macri, L., Casertano, S., et al. 2011, *ApJ*, 730, 119
- Ross, A. J., Ho, S., Cuesta, A. J., et al. 2011, *MNRAS*, 417, 1350
- Saito, S., Takada, M., & Taruya, A. 2008, *Physical Review Letters*, 100, 191301
- . 2009, *Phys. Rev. D*, 80, 083528
- . 2011, *Phys. Rev. D*, 83, 043529
- Scherrer, R. J., & Weinberg, D. H. 1998, *ApJ*, 504, 607
- Schulz, A. E., & White, M. 2006, *Astroparticle Physics*, 25, 172
- Schwetz, T., Tortola, M., & Valle, J. 2011
- Seljak, U. 1998, *ApJ*, 506, 64
- . 2000, *MNRAS*, 318, 203
- . 2001, *MNRAS*, 325, 1359
- Seljak, U., Slosar, A., & McDonald, P. 2006, *JCAP*, 0610, 014
- Seljak, U., et al. 2005, *Phys.Rev.*, D71, 103515, ja eprint =
- Seo, H.-J., Ho, S., & White, M. *et al.* 2012, submitted to *ApJ*
- Smith, R. E., Peacock, J. A., Jenkins, A., et al. 2003, *MNRAS*, 341, 1311
- Spergel, D., et al. 2003, *Astrophys.J.Suppl.*, 148, 175
- . 2007, *Astrophys.J.Suppl.*, 170, 377
- Swanson, M. E. C., Percival, W. J., & Lahav, O. 2010, *MNRAS*, 409, 1100
- Tegmark, M., Hamilton, A. J. S., Strauss, M. A., Vogeley, M. S., & Szalay, A. S. 1998, *ApJ*, 499, 555
- Tegmark, M., et al. 2004, *Phys.Rev.*, D69, 103501
- Thomas, S. A., Abdalla, F. B., & Lahav, O. 2010, *Phys.Rev.Lett.*, 105, 031301
- White, M., Blanton, M., Bolton, A., et al. 2011, *ApJ*, 728, 126
- York, D. G., Adelman, J., Anderson, Jr., J. E., et al. 2000, *ApJ*, 120, 1579